

# Phase Shift Modulation and DC-Link's Voltage Balancing Control for a DAB DC-DC Converter

Gedeon Niyitegeka\*, Elysee Malon Harerimana\*, Gawoo Park\*

\*R&D Center, Design Team  
G-Philos Company Ltd  
Yongin, South Korea

Jacho Choi\*\*†  
\*\*School of Electrical Engineering  
Chungbuk National University  
Cheongju, South Korea

**Abstract**— To improve the electrical energy consumption in modern transportation systems, a 1.5 kV DC bus in the future railway application has been considered by researchers and manufacturers. One of the preferred systems for this application is a high-frequency power electronics transformer to replace the existing 60 Hz power transformer. This solid-state transformer (SST) is made of multiple modules, and each module is composed of the AC/DC converter connected to a dual active bridge (DAB) DC-DC converter. A performing topology for the DAB is a three-level neutral point clamped (NPC) inverter on the left side and a two-level full bridge converter on the right side, both connected through a high-frequency isolation transformer. Due to its multilevel voltage on the primary side, its soft switching properties and the low number of components capability, the NPC based DAB converter is chosen to meet this smart transformer's requirements. This study proposes a novel control algorithm of the phase modulation and the voltage balancing perspective for future intelligent transformers.

**Keywords**—Phase shift, dual active bridge, smart transformer, neutral point clamped, voltage balancing.

## I. INTRODUCTION

Most of the current power systems are DC systems and AC systems combined together to strengthen the electrical energy sustainability in the world [1-3]. As the availability of renewable energy and regenerative energy becomes more prevalent, engineers and manufacturers have tried to integrate DC systems for several applications as a feasible solution in micro-grid technology. Therefore, to cope with the safe and efficient operation of AC and DC system together, there is always a need for power conditioning systems to make it [4-6]. To improve the power of traction motors, a high voltage solid state transformer (SST) for railway traction system was proposed and verified through the computer simulation [7].

This paper presents a resilient control algorithm for the DC/DC converter part of the SST shown in Fig. 1. The DC/DC converter side consists of the three parallel modules of the neutral point clamped (NPC) based dual active bridge (DAB) converter. The AC/DC converter side consists of three single-phase modules connected in cascade, but this part is not included in the current study.

Many frameworks about DAB have been published. A DAB DC/DC resonant converter with a generalized series and parallel resonant tank is analyzed [8]. To overcome the inrush current in the DAB DC/DC converter, the soft start algorithm plays a key role in system implementation [9, 10]. A DAB based bi- directional micro-inverter with the integrated short-term Li-ion ultra-capacitors storage and

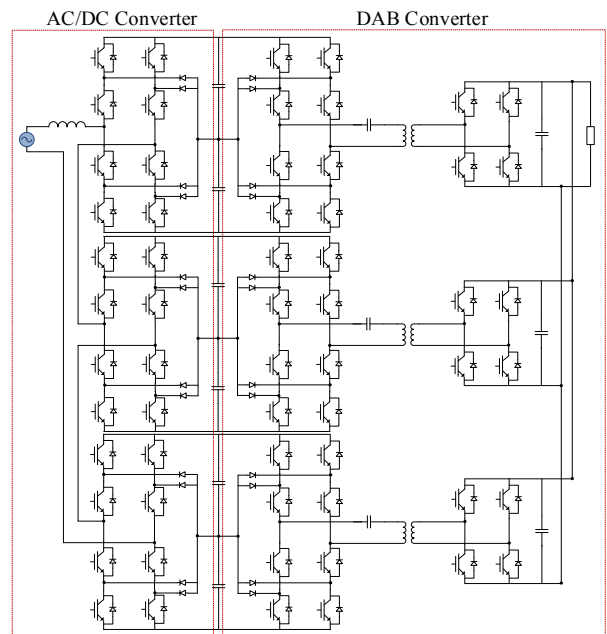


Fig. 1. 3-L NPC and single-phase cascade H-bridge intelligent transformer.

active power smoothing for photovoltaic application was studied [11]. In the bidirectional application, the control system of a DAB converter employs two different modulation schemes to deal with two operation scenarios characterized by the power flow direction. The bidirectional power flow capability of the DAB converter is only based on the phase shift between the primary and the secondary side voltages. In fact, the power flows from the leading voltage side to the lagging voltage side [12-14].

The analysis and design of a bi-directional DAB converter for fuel cell and super-capacitors hybrid UPS system showed that the mode conversion scheme should be used in the system to extend the zero voltage switching (ZVS) range and to improve the efficiency of the system [15, 16], but the control method and the control parameters should be deeply analyzed to enhance the system performance in the future applications.

In papers [17-18], the multilevel DAB DC-DC converter using symmetric phase shift modulation (PSM) was analyzed. To realize the five-level voltage on the primary of the transformer, the switching pulses and the resulting voltage waveforms were defined with respect to the angular distances, not to the duty ratio.

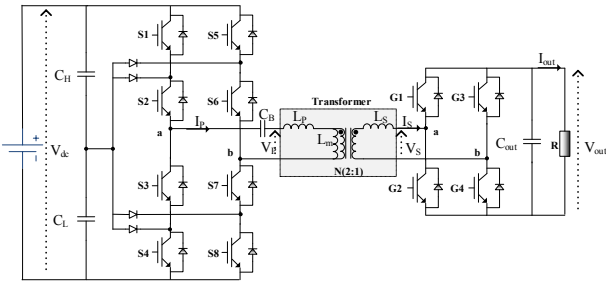


Fig. 2. NPC based DAB converter topology.

This paper is organized as follows: Section II presents and explains the topology configuration and modulation system of the NPC based DAB converter. Section III describes the design of a control algorithm proposed by this study to regulate the output voltage and to maintain the balance of the voltage of DC-link capacitors. Section IV contains the simulation results of the system, and the conclusions are made in section V.

## II. TOPOLOGY CONFIGURATION AND MODULATION METHOD

### A. Circuit details

A performing topology in consideration is a three-level NPC bridge converter and a two-level full bridge converter coupled by a high-frequency isolation transformer. It was recommended to use the three-level topologies in high voltage application because they offer a half DC voltage stress to the semiconductor devices [18-21]. The DAB DC/DC converters present the great behaviors in DC to DC power conversion due to its low number of components and high converting efficiency.

Fig. 2 represents a basic single module of a DAB DC/DC converter considered in this study. In this topology on the primary side of the transformer, the power stage is composed of the NPC single-phase bridge consisting of eight switching modules (IGBTs S1~S8), four clamping diodes, a blocking DC capacitor, and the two input capacitors. A blocking DC capacitor is used to protect the transformer against any DC current that may flow through the transformer from the NPC bridge side. On the secondary side of the transformer, the power stage is composed of four switching modules (IGBTs G1~G4) forming a two-level full bridge and one output capacitor. The parameters of the transformer and those of the DAB modules used in the simulation for this study are shown in Table I and Table II, respectively. The design process for the DC-link capacitors is described by the flowchart in Fig. 3.

### B. Paralleling modules

As the case study, a 75 kVA high-frequency SST system composed of three modules, each with 25 kVA, is considered. The voltage imbalance of the modules that may happen due to the arrangement of the AC/DC converter modules is predetermined by the studies of design analysis. Even though the control design system of the AC/DC converter includes the voltage balancing techniques, there is a high probability that the regulation of the DC-link voltage of all three modules connected in cascade may be unbalanced. Fig. 4 shows the DC-link voltages of the three parallel modules without and with the voltage balancing control to show the effect of having a voltage balancing controller in the control system of the DAB converter. This paper proposes the voltage balancing control algorithm for the control system of the DAB converter to suppress the voltage unbalance of capacitors and the voltage unbalance of modules as well.

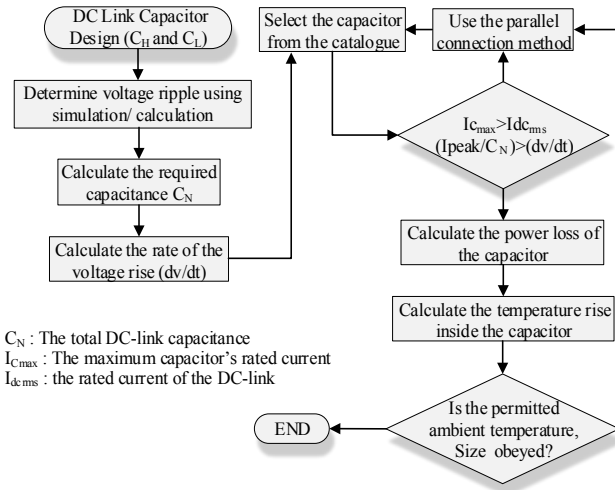


Fig. 3. Flowchart for selection of DC-link capacitor.

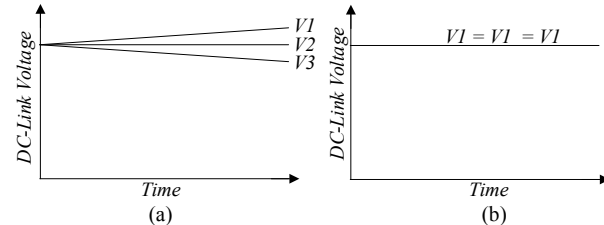


Fig. 4. DC link voltages of parallel modules: (a) Without balancing control, (b) with balancing control.

TABLE I. PARAMETERS OF TRANSFORMER

Parameter	Value
Magnetizing Inductance ( $L_m$ )	138.88 mH
Primary Leakage Inductance ( $L_p$ )	1.71 mH
Secondary Leakage Inductance ( $L_s$ )	413 uH
Turn ratio (N)	2:1

TABLE II. PARAMETERS OF DAB MODULE

Parameter	Symbol	Value
DC-Link Voltage	$V_{dc}$	1800 [V]
Link Capacitors	$C_H, C_L$	0.87 [mF]
Blocking Capacitor	$C_B$	25 [ $\mu$ F]
Output capacitor	$C_{out}$	0.68 [mF]
Output Voltage	$V_{out}$	750 [V]
Output Rated Current	$I_{out}$	33.3 [A]
Load	R	22.5 [ $\Omega$ ]
Switching frequency	$F_{sw}$	5 [kHz]
Alpha, Beta	$\alpha, \beta$	10°, 30°

TABLE III. SWITCHING PATTERN OF ONE LEG OF NPC

NPC Switching pattern			
S <sub>1</sub>	S <sub>2</sub>	S <sub>3</sub>	S <sub>4</sub>
1	1	0	0
0	1	1	0
0	0	1	1

### C. Modulation method

From the top to the bottom, the switching devices (IGBTs) of the leg (a) are named as S<sub>1</sub>, S<sub>2</sub>, S<sub>3</sub>, and S<sub>4</sub>, respectively. In the same way, the switching devices (IGBTs) of the leg (b) are named as S<sub>5</sub>, S<sub>6</sub>, S<sub>7</sub>, and S<sub>8</sub>, respectively.

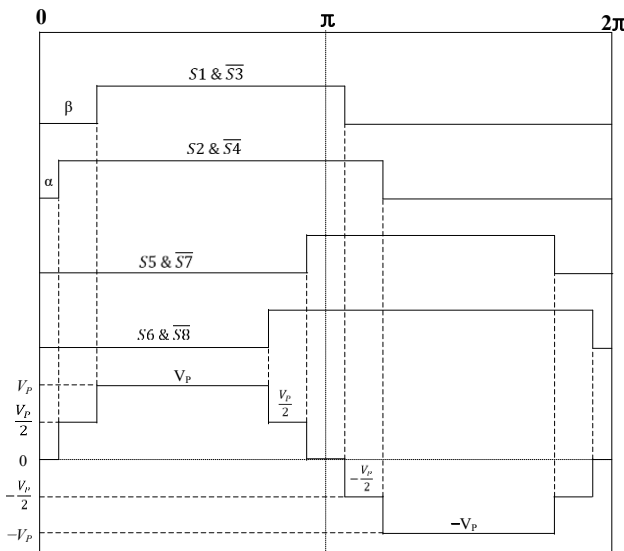


Fig. 5. NPC inverter gating signals and its output signal.

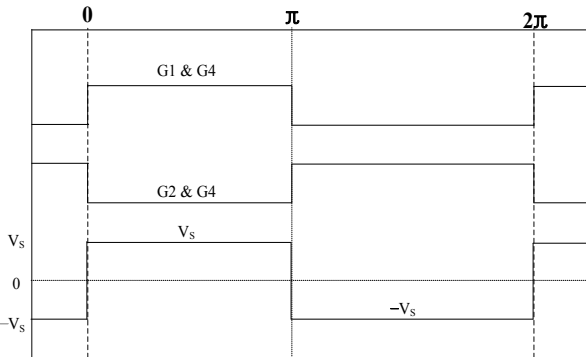


Fig. 6. Two-level converter gating signals and its input signal

There are various modulation schemes for NPC inverters and many researchers have proven the switching patterns which are suitable for NPC inverter in the DC-DC application.

The three switching states are defined by the NPC switching pattern. Table III shows the switching states of the leg (a) of a three-level NPC inverter. The gates  $S_1$  and  $S_3$  are complementary switched, and the gates  $S_2$  and  $S_4$  are complementary switched, too. The complementary switching modules are never switched at the same time. The leg (b) is modulated by the identical switching signals except that the phase shift is applied.

Therefore, to realize the five-level voltage at the primary of the transformer ( $V_p$ ), the switching pulses refer to both the initial phase angles ( $\alpha$  and  $\beta$ ), and the phase delay between legs a and b of the NPC inverter. The angles  $\alpha$  and  $\beta$  are the fixed delay applied to the NPC pulse width modulation (PWM) to be able to get a symmetrical multilevel signal on the output of the NPC. In principle, they enable the primary side voltage signal to pass throughout five voltage levels ( $V_p$ ,  $V_{p/2}$ , 0,  $-V_{p/2}$ ,  $-V_p$ ) for each switching half cycle as it is represented in Fig. 5. For one direction of the power flow, these angles are limited from 0 to  $\pi/2$  by respecting the conditions given in equation (1).

$$\begin{cases} 0 \leq \alpha < \frac{\pi}{2} \\ 0 < \beta \leq \frac{\pi}{2} \\ \alpha < \beta \end{cases} \quad (1)$$

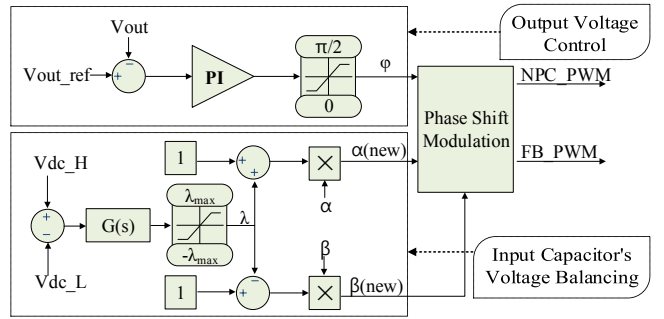


Fig. 7. Block diagram of output voltage control and voltage balancing control of input capacitors.

The secondary side is a two-level full bridge converter. Depending on the switching pattern, the gates  $G_1$  and  $G_2$  are complementary switched, and the gates  $G_3$  and  $G_4$  are complementary switched, too. The switching pattern for each IGBT consists of only two states. The input pulse has two voltage levels ( $V_p$ ,  $-V_p$ ). However, in some cases, the input pulse becomes a three voltage levels ( $V_p$ , 0,  $-V_p$ ) when a phase delay modulation between the legs of the full bridge converter is applied. Fig. 6 represents the switching and the input signals of a two-level full bridge converter.

### III. DESIGN OF CONTROL ALGORITHM

For DAB converters, the power transfer from one bridge to another needs a phase delay  $\varphi$  between two bridges. The power flows from the voltage leading bridge to the voltage lagging bridge. In addition, the maximum power of a DAB DC-DC converter is transferred when  $\varphi$  is equal  $\pi/2$ , and of course, when  $\varphi$  becomes negative. This means that the power is being transferred in opposite direction.

Fig. 7 shows the block diagram of the switching signals of NPC bridge for the voltage balancing control of the input capacitors and those of the two-level full bridge for the control of the output voltage. In the conventional control system, the switching signals of the NPC bridge are fixed during the operation, but this paper proposes a method to modify smoothly these PWM signals to eliminate the voltage unbalance in the system as clarified by the voltage balancing control loop part.

#### A. Output voltage control

The key to the stability and precision of the power conditioning systems is the performance of the controller. Using PWM signals, the switching elements are modulated and enabled to convert the input voltage into a desired output voltage. As shown in Fig. 7, the output voltage control loop compares the output voltage and the reference output voltage, and then the difference undergoes a PI control. The result is sent to the limiter to generate the required phase-shift magnitude  $\varphi$  and PWM signals. The phase angle  $\varphi$  varies dependently to the output power variation of the DAB DC/DC converter to maintain the desired output voltage level given as a reference, and it is applied between the PWM of the right side and the left side bridges.

#### B. Voltage balancing of capacitors

The voltage balancing control loop compares the sensed values of the DC-link top and bottom voltages after being filtered. And then, the difference between them is compensated by a particular compensator  $G(s)$ , and it generates the voltage balancing factor,  $\lambda$ , of input capacitors.

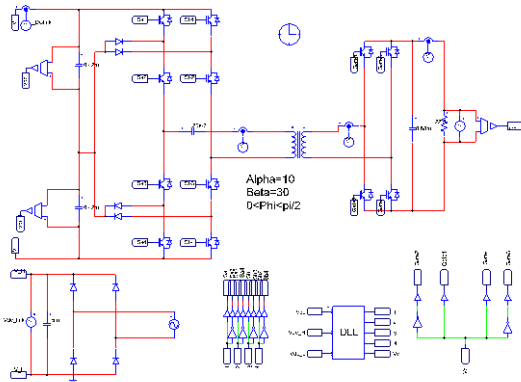


Fig. 8. The NPC based DAB converter module - PSIM schematics.

The equations of (2) and (3) explain the transfer function of the compensator  $G(s)$  and the voltage balancing factor,  $\lambda$ , respectively.

$$G(s) = K_1 \left( T_s + \frac{1}{K_2} \right) \quad (2)$$

$$(V_{dc-H} - V_{dc-L}) \times G(s) = \lambda \quad (3)$$

The voltage balancing factor is used to modify the initially fixed angles,  $\alpha$  and  $\beta$ , to keep the balance of the voltage of input capacitors. The voltage balancing factor band is determined by fulfilling the conditions given in equation (1). Therefore, having the defined values of the angles  $\alpha$  and  $\beta$  the voltage balancing factor range can be found by solving equation (4).

$$\begin{cases} (\lambda + 1) \times \alpha < (-\lambda + 1) \times \beta \\ (\lambda + 1) \times \alpha > 0 \\ (-\lambda + 1) \times \beta < \frac{\pi}{2} \end{cases}$$

It is then necessary to select the voltage balancing limiter  $\lambda_{max}$  from the entire solutions of equation (4). The limiter  $\lambda_{max}$  plays a key role to find the constants of the compensator,  $K_1$  and  $K_2$ .

For example, if  $\alpha=10$  and  $\beta=30$ , by solving the equation (4), the voltage balancing factor range is found as  $\lambda \in [-1, 0.5]$ . If the maximum tolerable voltage error to be balanced is given as  $\Delta V$ , then the constants,  $K_1$  and  $K_2$ , can be found using equations (5) and (6), respectively, where  $T_s$  is the sampling time, and  $\omega_n$  is the bandwidth of the compensator.

$$K_1 = \frac{1}{3} \times \Delta V \times T_s \times \omega_n \quad (5)$$

$$K_2 = \frac{1}{3} \times \left( \frac{\lambda_{max}}{\Delta V \times K_1} - T_s \right) \times 100 \quad (6)$$

#### IV. SIMULATION RESULTS

The PSIM software is used as the tool to perform the simulation. The simulation results of the DAB DC/DC converter are discussed to verify the validity of the proposed control algorithm. Fig. 8 shows the simulation schematics of one DAB module for 25 kVA. The simulation parameters are same as those given in Table I and Table II.

##### A. Voltage and phase control results

Typically, the output voltage regulation employs a technique of a fixed high-frequency PWM. In the simulation, the control system is designed and enabled to supervise the switching operation of the power stage to regulate the output voltage from the no-load to the maximum load power.

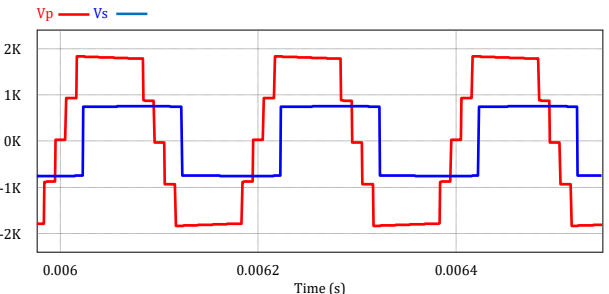
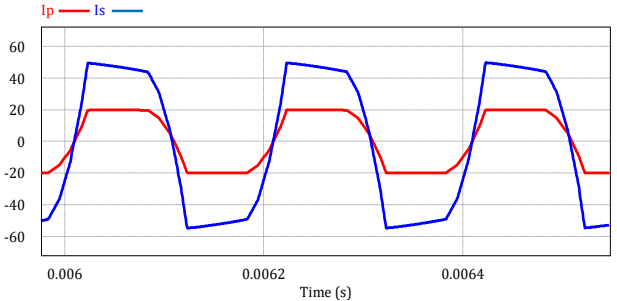
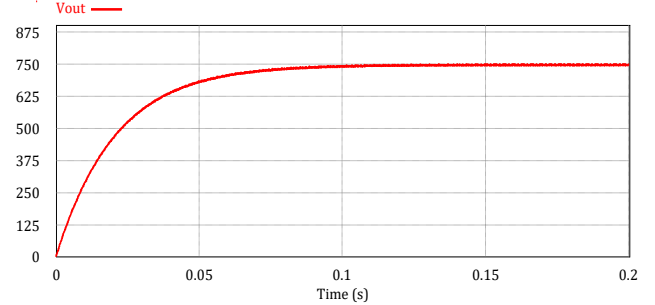
Fig. 9. The simulation waveforms of the voltage across the transformer ( $V_p$  and  $V_s$ ).Fig. 10. The simulation waveforms of the current across the transformer ( $I_p$  and  $I_s$ ).

Fig. 11. The simulation waveforms of the output voltage.

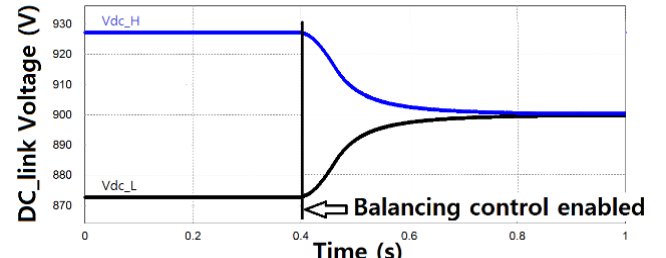
Fig. 12. The simulation results of  $V_{dc\_H}$  and  $V_{dc\_L}$  before and after balancing.

Fig. 9 represents the voltage waveforms of the primary side voltage,  $V_p$ , and the secondary side voltage,  $V_s$ , of the transformer. It can be clearly observed that  $V_p$  leads  $V_s$  by a phase delay  $\varphi$ . At no-load, the phase angle  $\varphi$  is almost null. The output voltage is controllable for the phase delay which is less than or equal  $\pi/2$ . Fig. 10 represents the waveforms of the primary current,  $I_p$ , and the secondary current,  $I_s$ , of the transformer. The accuracy of the output voltage control system is shown by the waveform of Fig. 11. The desired output voltage is 750 V, the regulator makes it precisely. The feedback is brought definitely to the desired value.

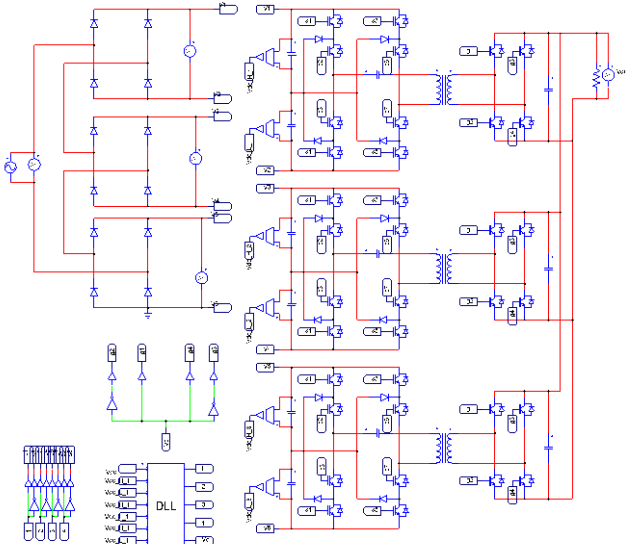


Fig. 13. PSIM schematics of three DAB modules in parallel.

### B. Voltage balancing of capacitors

Ideally, the input capacitors must have the same voltage values in normal conditions, even if there may be a difference, the few percentages of tolerance can be acceptable for many applications.

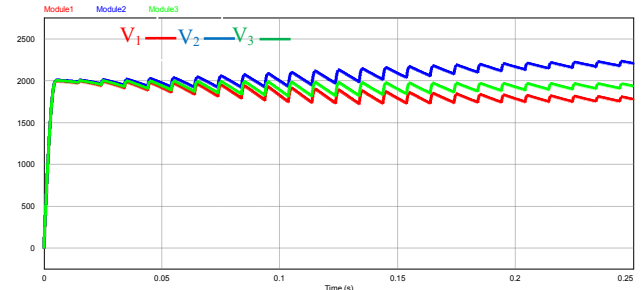
Therefore, with the conventional control systems for this NPC based DAB converter, the operation results in the voltage unbalance which cannot be tolerable for any application. Thus, in this study, the voltage balancing control algorithm of input capacitors is adopted.

To verify the performance of the proposed control algorithm for the voltage error recovery of input capacitors, the simulation is also performed, and the results are represented in Fig. 12. The voltage waveforms of input capacitors,  $V_{dc\_H}$  and  $V_{dc\_L}$ , are shown before and after enabling the voltage balancing control of input capacitors at 0.4s in the simulation. The results show that before activating the voltage balancing controller, the unbalance is about 6.2%, but the controller bounces back the error in less than two seconds after the activation of the voltage balancing controller and the voltages of two capacitors become evidently same.

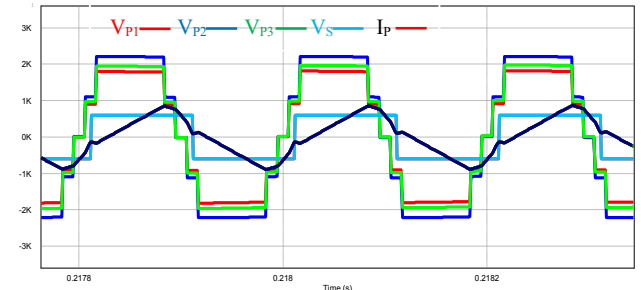
### C. Voltage balancing of modules

Fig. 13 is the simulation schematics of the three-parallel converters in PSIM. For the algorithm design of this smart transformer, three parallel DAB converter modules are supposed to be connected to three AC/DC converters arranged in cascade. Therefore, to create a similar situation, the three rectifying diode bridges are arranged in cascade to replace the AC/DC converter modules for simply analyzing the behaviors of the DC/DC converter part. Fig. 14 represents the simulation results without balancing control. The input DC voltage waveform of each module is shown in Fig. 14(a), the multilevel voltage behavior of each module are shown in Fig. 14(b). Since the corresponding input DC voltages of modules are unbalanced, the primary voltages are also totally unequal.

Therefore, it is a great move to consider the balancing controller in the control system of the NPC based DAB converter part to fortify the balancing control capacity of the

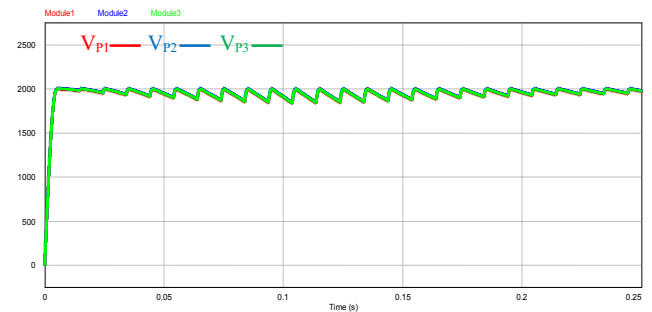


(a)

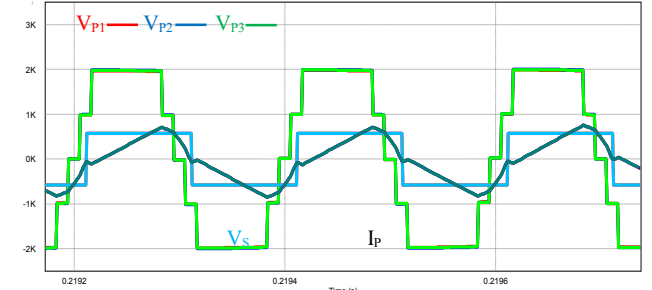


(b)

Fig. 14. Simulation results without balancing control: (a) DC-Voltage at the input of each module  $V_1$ ,  $V_2$  and  $V_3$ , (b) primary voltage across the transformers for all 3 modules,  $V_{p1}$ ,  $V_{p2}$ , and  $V_{p3}$ , secondary voltage,  $V_s$ , and the primary current,  $I_p$ .



(a)



(b)

Fig. 15. Simulation results with balancing control: (a) The DC-Voltage at the input of each module  $V_1$ ,  $V_2$  and  $V_3$ , (b) The primary voltage across the transformers for all 3 modules,  $V_{p1}$ ,  $V_{p2}$ , and  $V_{p3}$ , secondary voltage,  $V_s$ , and the primary current,  $I_p$ .

system. Fig. 15 represents the simulation results with balancing control to show the effect of the proposed voltage balancing control algorithm of input capacitors. From the simulation results, it is verified that the DAB DC/DC converter needs the DC-link balancing control to cope with the voltage imbalance of associated capacitors and the system control is very stable and efficient.

## V. CONCLUSIONS

In this paper, the switching system of NPC based BAD DC-DC converter is explained. The theoretical analysis of control and the considerations for algorithm design are discussed and verified by the simulation results. This study proposes a novel method to modulate the gates of DAB converters and explains the voltage balancing control method of input capacitors. The control system presents a great performance dealing with the DC-link voltage unbalance issue of the modules and provides a reliable operation. The simulation results proved that three-level NPC based DAB converters are a great candidate for the projected SST system and for high voltage application as well.

## ACKNOWLEDGMENT

This work was supported by the research project fund of the Ministry of Trade, Industry, and Energy (South Korea) and the Korea Institute of Energy Technology Evaluation and Planning (KETEP) under the grant number 20173010140890.

## REFERENCES

- [1] A. Lachuriya and R. D. Kulkarni, "Stationary electrical energy storage technology for global energy sustainability: A review," *Proc. of IEEE ICNTE'2017*, pp. 1-6, Jan. 2017.
- [2] M. Farhadi and O Mohammed, "Energy storage technologies for high power applications," *IEEE Trans. on Ind. Appl.*, vol. 52, no. 3, pp. 1953-1961, Jun. 2016.
- [3] G. Niyitegeka, J. Choi and Y. Ok, "Improved droop control for effective load sharing and voltage regulation in DC microgrids," *Proc. of IEEE PQ'2016*, pp. 125-132, Aug. 2016.
- [4] S. Daher, J. Schmid, and F. L. M. Antunes, "Multilevel Inverter Topologies for Stand-Alone PV Systems," *IEEE Trans. on Ind. Electron.*, vol. 55, no. 7, pp. 2703-2712, Jul. 2008.
- [5] H. Li, Y. Iijima, and N. Kawakami, "Development of power conditioning system (PCS) for battery energy storage systems," *Proc. of ECCE Asia'2013*, pp. 1295-1299, Jun. 2013.
- [6] F. Gao, P. C. Loh, F. Blaabjerg, and D. M. Vilathgamuwa, "Performance evaluation of three-level z-source inverters under semiconductor-failure conditions," *IEEE Trans. on Ind. Appl.*, vol. 45, no. 3, pp. 971-981, June 2009.
- [7] S. Kim, S. Lee, and M. Kim, "Structure of Smart Transformer with Single Phase Three-Level H-Bridge Cascade for Railway Traction System," *J. of the Korean Society for Railway*, vol. 19, no. 5, pp. 617-628, 2016.
- [8] G. Y. Hu, X. Li, and B. Y. Luan, "A Generalized Approach for the steady-state Analysis of DUAL Active Bridge Resonant Converter," *Energies* 2014, pp. 7915-7935, 2014.
- [9] F. Giuliani, N. Delmonte, P. Cova, A. Costabeber, and A. Castellazzi, "Soft Start procedure for Dual Active Bridge Converter," *Proc. of IEEE COMPEL'2015*, pp.1-6, 2015.
- [10] H. Choi and J. Jung, "Practical Design of Dual Active Bridge Converter as Isolated Bidirectional Power Interface for Solid State Transformer Applications," *J. Electr. Eng. Technol.*, vol. 11, no. 5, pp. 1921-1929, 2016.
- [11] Y.C. Wang, F.M. Ni, and T.L. Lee, "Hybrid Modulation of Bidirectional Three-Phase Dual Active Bridge DC Converters for Electric Vehicles," *Energies* 2016, pp. 492-505, 2016.
- [12] M. T. Tsai, C. L. Chu, and W. C. Chen, "Implementation of a Serial AC/DC Converter With Modular Control Technology," *Proc. of IEEE ICRERA'2018*, pp.245-250, 2018.
- [13] N. Kimura, T. Morizane, I. Iyoda, K. Nakao and T. Yokoyama, "Solid state transformer investigation for HVDC transmission from offshore windfarm," *Proc. of IEEE ICRERA'2017*, pp. 574-579, 2017.
- [14] M. Rashidi, A. Nasiri and R. Cuzner, "Application of multi-port solid state transformers for microgrid-based distribution systems" *Proc. of IEEE ICRERA'2016*, pp. 605-610, 2016.
- [15] Z. Zhang, O. C. Thomsen, M. A. E. Andersen, J. D. Schmidt, and H. R. Nielsen, "Analysis and Design of Bidirectional DC-DC Converter in Extended Run Time DC UPS System Based on Fuel Cell and Supercapacitor," *Proc. of IEEE, APEC' 2009*, pp. 714-719, 2009.
- [16] S. Poshtkouhi, M. Fard, H. Hussein, L. M. D. Santos, O. Trescases, M. Varlan, and T. Lipin, "A Dual Active Bridge based Bidirectional Micro-Inverter with Integrated Short-Term Li-Ion Ultra-Capacitors Storage and Active Power Smoothing for Modular PV Systems," *Proc. of APEC'2014*, pp. 643-649, 2014.
- [17] M. A. Moonem, C. L. Pechacek, R. Hernandez, and H. Krishnaswami, "Analysis of a Multilevel Dual Active Bridge (ML-DAB) DC-DC Converter Using System Modulation," *Inter. J. Molecular Sc. - Electronics* 2015, pp. 239-260, 2015.
- [18] M. A. Moonem and H. Krishnaswami, "Analysis of a Multilevel Dual Active Bridge DC-DC Converter Using System Modulation," *Proc. of IEEE ECCE'2012*, pp. 1556-1561, 2012.
- [19] I. Ouerdani, A. B. B. Abdelghani and I. S. Belkhodja "Harmonic Analysis of Pulse Width Modulation-Based Strategies for Modular Multilevel Converter," *Proc. of IEEE IJRER'2016*, pp. 838-846, 2016.
- [20] R. R. Behera, A. N. Thakur "Hybrid Modular Multilevel Converter Based Single-Phase Grid Connected Photovoltaic System," *Proc. of IEEE IJRER'2017*, pp. 1245-1249, 2017.
- [21] S. B. Bahir, A.R. Beig and M. Poshtan "An improved space vector PWM for grid connected MMC," *Proc. of IEEE ICRERA'2017*, pp. 556-561, 2017.



**Gedeon Niyitegeka** received his B.S. degree from the Department of Electrical Engineering, Rwanda National University, Huye, Rwanda and M.S degree from the Department of Electrical Engineering, Chungbuk National University, Cheongju, South Korea, in 2013 and 2016 respectively. From 2016 till now, he is currently working as a Research Engineer at G-Philos Company Ltd, Yongin, South Korea.



**Elysee Malon Harerimana** received his B.S. degree from the Department of Electrical Engineering, Rwanda National University, Huye, Rwanda and M.S degree from the Department of Electrical Engineering, Jeonju University, Jeonju, Korea, in 2013 and 2016 respectively. From 2017 till now, he is currently working as a Research Engineer at G-Philos Company Ltd, Yongin, South Korea.



**Gawoo Park** received his B.S. degree from the Department of Electronics Engineering, Hanbat National University, Daejeon, Korea and M.S degree from the Department of Electrical Engineering, Chungbuk National University, Cheongju, South Korea, in 1992 and 1995 respectively. From 1994 to 2004, he was working at POSCO ICT Company Ltd, Pohang, South Korea, as a Senior Research Engineer. From 2004 to 2009, he was the Director of the Research Department at PLASPO, Goyang, South Korea. From 2009 till now, he is the Chief Executive Officer and the Director of the Research at G-Philos Company Ltd, Yongin, South Korea. His current research interests include the Power Electronic Systems, Renewable Energy, Energy Management Systems, Energy Storage Systems, and Fuel Cell Systems.



**Jaeho Choi** received his B.S., M.S., and Ph.D. degrees from the Department of Electrical Engineering, Seoul National University, Seoul, South Korea, in 1979, 1981, and 1989 respectively. From 1981 to 1983, he was a full-time Lecturer at Jungkyoung Technical College, Daejeon, South Korea. Since 1983, he has been with the School of Electrical Engineering at Chungbuk National University, Cheongju, South Korea, where he is currently a Professor. In 1993, 1998, 2003, and 2009, he was a Visiting Professor at the University of Toronto, Toronto, Canada. He was also a Danfoss Visiting Professor at the Aalborg University, Aalborg, Denmark, in 2000, and a Visiting Professor at the Bandung Institute of Technology, Bandung, Indonesia, in 2017. His current research interests include Power Electronics, Power Quality Problems and Solutions, Energy Storage Systems, and Renewable Energy in Microgrid Systems. He is an active member of KIEE, KIPE, and IEEE. He was the Editor-in-Chief of the JPE and the president of the KIPE.